Potential effects of the marine carbon cycle on the multiple equilibria window of the Atlantic Meridional Overturning Circulation

A. Boot[1], A. S. von der Heydt[1,2], and H. A. Dijkstra[1,2]

[1]Institute for Marine and Atmospheric research Utrecht, Department of Physics,Utrecht University, Utrecht, the Netherlands
[2]Center for Complex Systems Studies, Utrecht University, Utrecht, the Netherlands

Key Points:

- The marine carbon cycle can influence the multiple equilibria window of the Atlantic Meridional Overturning Circulation.
- Larger carbon content of the ocean-atmosphere system increases the size of the multiple equilibria window.
- The balance between sources and sinks of carbon and the coupling between the water cycle and atmospheric pCO_2 are controls for the multiple equilibria window.

Corresponding author: Amber Boot, `d.boot@uu.nl`

Abstract

The Atlantic Meridional Overturning Circulation (AMOC) is considered to be a tipping element in the Earth System with multiple stable states. Here, we investigate the multiple equilibria window of the AMOC within a coupled ocean circulation-carbon cycle box model. We show that adding couplings between the ocean circulation and the carbon cycle model affects the multiple equilibria window of the AMOC. Increasing the total carbon content of the system will widen the multiple equilibria window of the AMOC, since higher atmospheric pCO_2 values are accompanied by stronger freshwater forcing over the Atlantic ocean which acts to increase the window. Our results suggest that future changes in the marine carbon cycle can influence AMOC stability in future climates.

Plain Language Summary

The Atlantic Meridional Overturning Circulation (AMOC), an important circulation system in the Earth System, is considered to be a tipping element with multiple stable states. In this study we investigate the range in which these multiple stable states exist, termed the multiple equilibria window, with a simple coupled ocean circulation-carbon cycle box model. We show that depending on the coupling between the ocean circulation model and the carbon cycle model, the multiple equilibria window of the AMOC changes, where it can become both smaller and larger. Furthermore, we also show that when total carbon content in the ocean-atmosphere system is increased, the width of the multiple equilibria window is increased. These results suggest that the marine carbon cycle has influenced AMOC stability in past climates, and can influence it in future climates.

1 Introduction

The Atlantic Meridional Overturning Circulation (AMOC) transports heat from the Southern to the Northern Hemisphere and thereby plays a large role in modulating global climate (Vellinga & Wood, 2008; Palter, 2015). It is one of the prominent tipping elements in the Earth System (Lenton et al., 2008; McKay et al., 2022). Model studies suggest that the AMOC has multiple stable states: the on-state, representing the current AMOC state with a strong northward flow at the surface and a southward return flow at intermediate depth; and the off-state, representing a weak or even reversed AMOC state (Weijer et al., 2019). From a dynamical systems point of view, a bi-stable AMOC regime appears through the occurrence of two saddle node bifurcations (Dijkstra, 2007) and the region in parameter space where both on- and off-states co-exist is the multiple equilibria window (MEW), also referred to as the bi-stability window (Barker & Knorr, 2021).

Climate variability in the past, such as Heinrich events, has been linked to tipping of the AMOC (Rahmstorf, 2002; Lynch-Stieglitz, 2017). Under anthropogenic forcing, the global warming threshold for AMOC tipping has been recently estimated to be around 4 °C (McKay et al., 2022). Model data from the Coupled Model Intercomparison Project 6 (CMIP6; Eyring et al., 2016), Weijer et al. (2020) project a consistent weakening of the AMOC under future climate change, with a 34-45% decrease in AMOC strength in 2100, but no clear tipping was found. However, these models may have a too stable AMOC (Weijer et al., 2019) and the probability of AMOC tipping before 2100 may still be non-negligible. Under AMOC tipping, a strong cooling in the Northern Hemisphere (Rahmstorf, 2002; Drijfhout, 2015), changes in the water cycle (Vellinga & Wood, 2002; Jackson et al., 2015), and potential interactions with other tipping elements in the Earth System (Dekker et al., 2018; Wunderling et al., 2021; Sinet et al., 2023) are expected.

The AMOC can also interact with the marine carbon cycle and therefore influence atmospheric pCO_2. By affecting the transport of important tracers, such as dissolved

inorganic carbon (DIC), total alkalinity, and nutrients, the AMOC affects the solubility and biological carbon pumps. Evidence for a coupling between the AMOC and marine carbon cycle is provided in proxy data (Bauska et al., 2021). Model studies show a wide range of potential carbon cycle responses to a collapse of the AMOC. While most models show an increase in atmospheric pCO_2 (e.g. Marchal et al., 1998; Schmittner & Galbraith, 2008; Matsumoto & Yokoyama, 2013), the magnitude and precise mechanisms are dependent on the model used and climatic boundary conditions (Gottschalk et al., 2019).

As the AMOC can influence atmospheric pCO_2, there is a potential feedback mechanism since CO_2 influences the hydrological cycle (Weijer et al., 2019; Barker & Knorr, 2021) and, through changes in buoyancy fluxes, affects the AMOC. Previous studies suggest that there may be a relation between atmospheric pCO_2 and the MEW of the AMOC (Barker et al., 2010, 2015). However, a clear mechanistic view has not been given yet. Here, we study the mechanisms on how the marine carbon cycle affects the MEW of the AMOC using a coupled Atlantic Ocean circulation-carbon cycle box model.

2 Method

We couple an Atlantic Ocean circulation model (Cimatoribus et al., 2014; Castellana et al., 2019) to a carbon cycle model (O'Neill et al., 2019; Boot et al., 2022). The ocean circulation model (Fig. 1) simulates the distribution of salinity in 5 ocean boxes and the depth of the pycnocline in the Atlantic Ocean and is well suited to simulate AMOC dynamics (Cimatoribus et al., 2014). Salinity in the model is affected by wind and buoyancy driven ocean flows and by freshwater fluxes. The carbon-cycle model simulates DIC, alkalinity (Alk) and phosphate (PO_4) and captures relevant processes such as riverine input, air-sea gas exchange, biological export production, $CaCO_3$ rain, $CaCO_3$ dissolution and sediment burial (Fig. 1). The AMOC influences the carbon cycle directly by advective transport of the tracers and the simulated salt distributions in the AMOC model are used as input for the carbonate chemistry and tracer transport in the carbon-cycle model. An important coupling between both models is due to the fact that biological export production is dependent on nutrient transport. By representing the symmetrical component of the freshwater forcing E_s of the AMOC model (Fig. 1) as a function of atmospheric pCO_2, another important coupling between both models is represented.

To determine the functional relation between pCO_2 and E_s, we use a fit from a CMIP6 multi-model mean, based on 28 models, simulated under the 1% CO_2 increase scenario (Eyring et al., 2016). We fit both a linear and logarithmic function to atmospheric pCO_2 data and the freshwater flux into the ocean region represented by the thermocline box in our model (box t in Fig. 1). There is net evaporation over this region which represents $2 E_s$ in the box model resulting in the linear (Eq. 1) and logarithmic (Eq. 2) fits shown in Figure S1. We will use both fits in section 3.1 since the fits show different behavior for pCO_2 values lower than 300 ppm, and by using both we test the sensitivity of the model to the used fit. The fits (in Sv) are given by:

$$E_s = 0.562 + 0.00012 \times pCO_2 \tag{1}$$

$$E_s = 0.099 + 0.079 \times \ln(pCO_2) \tag{2}$$

Both relations above capture the effect of CO_2 induced warming on the hydrological cycle that results in the subtropical regions becoming drier under higher pCO_2 values, while sub-polar regions become wetter, which is indeed seen in both model and paleo proxy studies (Held & Soden, 2006; Bonfils et al., 2020; van der Ploeg et al., 2023).

The relations (Eq. 1) and (Eq. 2) could only be determined from the CMIP6 models over a limited range of $p(CO_2)$ and only for time varying climates. To extend that
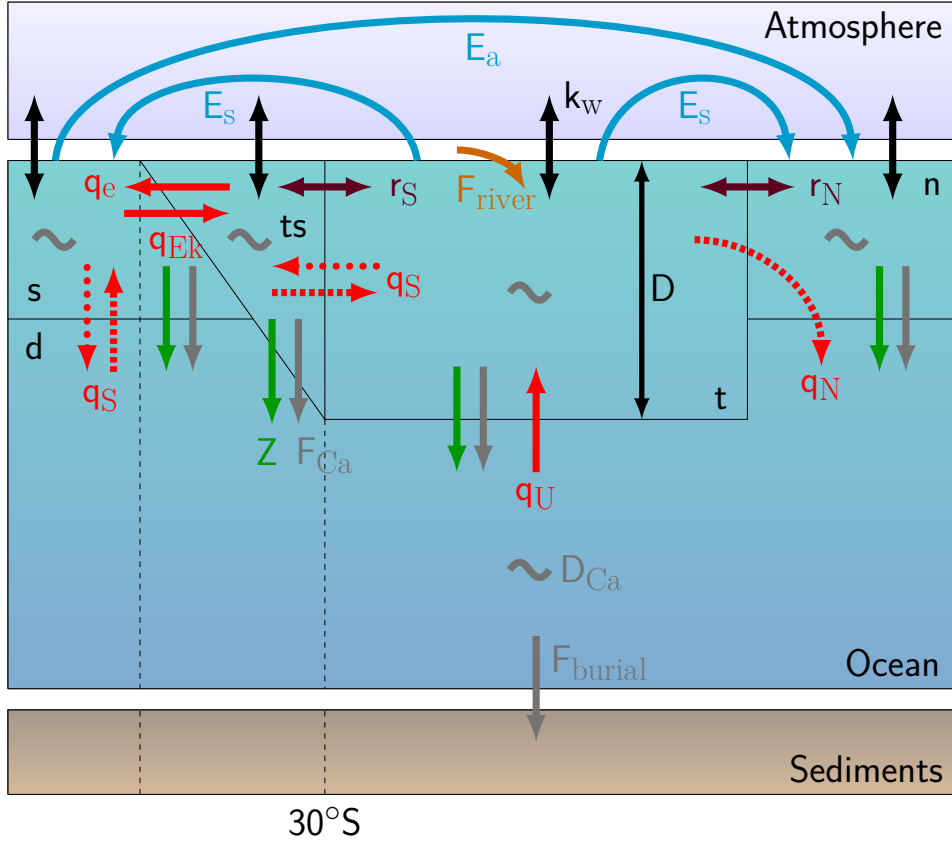
Figure 1. Box structure and processes simulated in the coupled circulation – carbon cycle model. Red arrows represent volume transports where dashed arrows are only present during an on-state, and dotted arrows only present during an off-state. The purple arrows represent gyre exchange (r_N and r_S), and blue arrows freshwater fluxes (E_s for the symmetrical forcing, and E_a for the asymmetrical forcing). Carbon cycle processes that are represented are riverine input (orange), air-sea gas exchange (black; k_w), biological export production (green; Z), $CaCO_3$ rain (grey; F_{Ca}), $CaCO_3$ dissolution (grey; D_{Ca}), and sediment burial (grey; F_{burial}). Based on Castellana et al. (2019) and Boot et al. (2022).

range and to capture the possibility that the fits (Eq.1 and 2) do not accurately represent the E_s-pCO_2-coupling in steady state climates, we also use a third relation

$$E_s = 0.1 + 0.75 \times \ln\left(\frac{pCO_2 + 250}{pCO_{2,0}}\right) \tag{3}$$

to demonstrate the effect of the carbon cycle on the AMOC MEW for a larger range of possible E_s-pCO_2 coupling strengths. The parameter values in (Eq. 3) are tuned such that E_s approaches 0 when atmospheric pCO_2 approaches 0, and that $E_s = E_{s,base}$ (0.56 Sv) when atmospheric pCO_2 is equal to $pCO_{2,0} = 300$ ppm. When the CO_2 concentration exceeds $pCO_{2,0}$, E_s will be larger than $E_{s,base}$. Both logarithmic fits (Eq. 2 and Eq. 3) are used in sections 3.1 and 3.2.

3 Results

The equations of the coupled model (see Supporting Information) are implemented in the continuation software AUTO-07p (Doedel et al., 2007), which is able to efficiently compute branches of steady state solutions in parameter space and to detect the saddle-node bifurcations bounding the MEW. For the AMOC bifurcation diagram, we use the asymmetric component of the freshwater flux E_a as a control parameter as in Castellana et al. (2019). In the results below, we will consider four different cases of the model related to capturing different carbon-cycle processes. In case REF we use the default coupled circulation-carbon cycle model. In BIO we add the coupling of export production to the ocean circulation. In BIO+E_s, the E_s-pCO$_2$ coupling is added, and lastly, in case BIO+E$_s$+FCA, the rain ratio is modelled as a function of the calcium carbonate (CaCO$_3$) saturation state, whereas in the other three cases it is constant (see also Table S1 for the specifics of the different cases).

3.1 The AMOC multiple equilibria window

The bifurcation diagrams, showing the AMOC strength versus E_a are for the three E$_s$-pCO$_2$ relations (Eq. 1), (Eq. 2) and (Eq. 3) in Fig. 2a-b, Fig. 2c-d and Fig. 2e-f, respectively.

To be able to simulate both the on- and off-branch in the coupled model, it is vital that the BIO coupling is used, since otherwise phosphate concentration in the surface ocean will become negative under a collapsed AMOC regime. This behavior is illustrated in Fig. 2a, b by the cases REF and BIO. In case REF the off-branch is not shown, while for case BIO the full bifurcation diagram with two saddle-node bifurcations is plotted. Atmospheric pCO$_2$ also shows hysteresis behavior with low concentrations on the off-branch (around 50 ppm).

To explain the low pCO$_2$ values on- the off-branch we look at the constraint in the model on total carbon content in the ocean-atmosphere system. In steady state, the riverine input and sediment outflux of DIC must balance to keep the total carbon content constant (in time). In our model, the sediment outflux is a function of the saturation state of CaCO$_3$ and CaCO$_3$ flux which is a function of the rain ratio (constant in non-FCA cases) and the export production. However, in this model set up, the saturation state of CaCO$_3$ in the ocean is in every box larger than 1, meaning that there is no saturation driven dissolution of CaCO$_3$ and the sediment outflux is purely a function of the export production. In an AMOC off-state, nutrient advection is low causing a large reduction in export production, and therefore a small sediment outflux. The riverine influx must balance this small outflux, which can only be achieved by decreasing atmospheric pCO$_2$ to the values reported on the off-branch. When the rain ratio feedback is used (case FCA), this mechanism is also present, but the sediment outflux is in this case also a function of the rain ratio. In the FCA case, the rain ratio is variable when the saturation state of CaCO$_3$ is larger than 1. This results in larger rain ratio values, and therefore more CaCO$_3$ export to the sediments increasing the sediment outflux and, through the river influx, atmospheric pCO$_2$.

When the linear CMIP6 E$_s$-pCO$_2$ coupling (Eq. 1) is used, the MEW increases slightly. The saddle node on the on-branch shifts from 0.45Sv to 0.46Sv, and the saddle node on the off-branch shifts from -0.08Sv to -0.10Sv for both E$_s$+BIO and E$_s$+BIO+FCA. Due to the presence of a subcritical Hopf bifurcation in the AMOC model, the on-branch becomes unstable before the saddle node. The presence of the Hopf bifurcation is not further considered in this study as we are only interested in the MEW. The small movement of the saddle nodes in parameter space shows that when the linear CMIP6 fit is used, the CO$_2$ dependency of E$_s$ is too weak to significantly impact the MEW. When the logarithmic CMIP6 fit (Eq. 2) is used, the MEW becomes smaller (Fig. 2c, d). The logarithmic fit (Eq. 3) over the full pCO$_2$ range shows that the marine carbon cycle can

have a substantial effect on the AMOC MEW, as the saddle node on the off-branch moves to larger values of E_a.

To explain the movement of the saddle nodes, we consider the sensitivity of the model to E_s (Figure S1). The default value used for cases REF and BIO for E_s is 0.56 Sv. The logarithmic CMIP6 fit results in a slightly smaller value, whereas the linear fit has a slightly larger value. Due to increased E_s, the thermocline becomes saltier, and in combination with the salt-advection feedback, this leads to a larger meridional density gradient and therefore a stronger AMOC. Furthermore, increased E_s increases the net evaporation over the Atlantic, given by (E_s-E_a) and a larger E_a is necessary to tip the AMOC. On the off-branch, a larger E_s results in salinification of the *ts* box and a more negative fresh-water flux (E_a) is needed to increase the meridional density gradient and reinvigorate the AMOC. This behavior of the AMOC model explains the differences between Figs. 2a-b and 2c-d. The fit Eq. 3 narrows the MEW by moving the saddle node on the off-branch to larger values of E_a (Fig. 2e, f). Using this fit shows more clearly that there can be an influence on the MEW via a coupling to atmospheric pCO_2. Here, it reduces the MEW by moving the off-branch saddle node to larger values of E_a which can be explained by the fact that CO_2 on the off-branch is smaller than $CO_{2,0}$ and therefore E_s is smaller than $E_{s,base}$.

3.2 Sensitivity to total carbon content

Over the Cenozoic, both the AMOC (Lynch-Stieglitz, 2017) and total carbon content in the ocean-atmosphere system have varied (Zeebe et al., 2009; Caves et al., 2016). In Caves et al. (2016) it is suggested that total carbon content has varied between 24,000 PgC and 96,000 PgC. In the previous section, the model was studied with approximately 8000 PgC in the Atlantic and Southern Ocean which translates to approximately 40,000 PgC in the global system (since our model represents approximately 20% of the global ocean). In this section, we analyze how the sensitivity to E_a changes under different total carbon contents in the model. To test the sensitivity, we remove approximately 2000 (-25%) PgC, and add approximately 2000 (+25%), 4000 (+50%) and 8000 (+100%) PgC. We do this for the CMIP6 logarithmic coupling (Eq. 2; Fig. 3a-c) and the strong logarithmic coupling (Eq. 3; Fig. 3d-f). Both cases show similar results, but in Fig. 3a-c the MEW changes are less pronounced; we therefore focus on the results in Fig. 3d-f.

The MEW increases when total carbon increases. There is, however, a different response when the rain ratio feedback (FCA) is included. For case E_s+BIO we see that the MEW increases under a total C change from -2000 PgC to +2000 PgC, but then remains constant for more carbon content. We can explain this by looking at the atmospheric pCO_2 values, and therefore also E_s, at the saddle node, which are similar for the three high carbon cases. When the rain ratio feedback is used, we see that the MEW keeps increasing for larger carbon contents since also the atmospheric pCO_2 increases. We can explain the difference between E_s+BIO and E_s+BIO+FCA by the constraint on total carbon in the ocean-atmosphere system. In E_s+BIO, biological export production is mainly a function of the AMOC strength, whereas in the E_s+BIO+FCA case it is also dependent on the $CaCO_3$ saturation state which is coupled to atmospheric pCO_2 through the pH of the surface ocean. This increases the biological export production, and through the same mechanisms as described before, higher atmospheric pCO_2 values.

4 Summary and discussion

In this paper we investigated the multiple equilibria window (MEW) of the AMOC in a coupled ocean circulation-carbon cycle box model. When freshwater forcing is coupled to atmospheric pCO_2 using CMIP6 multi-model fits (Eq. 1 and Eq. 2), the MEW changes slightly due to a weak dependency on atmospheric pCO_2. However, when we use a stronger coupling (Eq. 3), the saddle node on the off-branch moves towards larger

E_a values and thereby reduces the MEW. We also assessed the sensitivity to total carbon content in the system and found that the MEW is larger with more carbon in the system due to a shift of both the on- and off-branch saddle nodes. Both results show the potential of the marine carbon cycle to influence the MEW of the AMOC.

We acknowledge that it is difficult to provide an adequate justification of the different E_s-pCO$_2$ relations because the CMIP6 model pCO$_2$ range is too small and there are no observations which can test the strong coupling relation (Eq. 3). However, from the results clear and plausible mechanisms can be extracted which cause the change in MEW and these are more important than the precise quantitative estimates. Two processes explain the results on the MEW: (1) the balance between the river flux and sediment flux that constrains atmospheric pCO$_2$; and (2) the sensitivity of the AMOC to E_s. In the model, atmospheric pCO$_2$ is dependent on the ocean circulation through export production, E_s is dependent on atmospheric pCO$_2$, and the ocean circulation is dependent on E_s, creating a feedback loop (Fig. 4). We see that when atmospheric pCO$_2$ is high, so is E_s which results in a stronger AMOC on the on-branch. As a consequence, export production is increased and there will be a larger outflux of carbon and alkalinity through the sediments, which is balanced by a high influx of carbon through the rivers, consistent with high atmospheric pCO$_2$ values. Of the feedbacks that we have implemented, only the rain ratio feedback (FCA) affects this mechanism because it directly influences the sediment outflux and makes the carbon cycle less sensitive to the ocean circulation.

The results here can be relevant when studying climate transitions in past and future climates as it identifies mechanisms how AMOC stability can depend on background climate and atmospheric pCO$_2$ values. Previous work focused on the Pleistocene suggest an influence of atmospheric pCO$_2$ on the stability structure of the AMOC through temperature (Sun et al., 2022) and moisture transport (Zhang et al., 2017). In our model, there is no effect of temperature changes, but the E_s coupling used here is similar to the moisture transport described in Zhang et al. (2017) the only difference being that this moisture transport is to the Pacific basin, whereas in our model it is redistributed over the Atlantic to conserve salinity.

We have used a model that provides a simple framework for studying AMOC dynamics that allows us to efficiently test the concept of AMOC stability in a wide range of parameter values. However, a limitation is that the model only represents a fifth of the global ocean, the Atlantic and Southern Ocean. For the circulation model this might not be a large deficiency, but for the carbon cycle model it might be. Furthermore, the coupled model might not be valid for the entire parameter space we have simulated. An example of this, is the unrealistic low pCO$_2$ values on the off-branch. These low values suggest that some important processes are missing, e.g. negative feedbacks arising in the Indo-Pacific basin or in the terrestrial biosphere. Though not a limitation in the model, it is good to note that the range of timescales in the carbon cycle model is larger than in the circulation model, which does not affect our results but does affect the time dependent response of the system.

Our work also holds implications for assessing AMOC stability in future climates. Currently, the global warming threshold for an AMOC collapse is estimated to be 4 °C (McKay et al., 2022). In the future, the carbon content of the ocean-atmosphere system will increase, potentially increasing the MEW which can change the likelihood of a bifurcation induced AMOC collapse. In this study we focused on slow, bifurcation induced tipping of the AMOC, while the AMOC is also able to tip due to faster processes resulting in noise-induced tipping (Castellana et al., 2019). We hope this work inspires further research on the dependency of the MEW of the AMOC on the carbon cycle in more detailed models to further investigate the relevance of the mechanism found in this study and provide a quantification for the influence of the marine carbon cycle on the MEW of the AMOC.

Appendix A   Open Science

Model code, generated model data, scripts for plotting all figures can be found at `10.5281/zenodo.8042693` (Boot et al., 2023). A list of used datasets, processed datasets and citations for the CMIP6 multi-model fits is also included in this repository. CMIP6 model data can be downloaded from the Earth System Grid Federation (ESGF) (`https://esgf-node.llnl.gov/search/cmip6/`). AUTO-07p can be downloaded from `https://github.com/auto-07p`.

References

Andersson, A., Graw, K., Schröder, M., Fennig, K., Liman, J., Bakan, S., . . . Klepp, C. (2017). *Hamburg Ocean Atmosphere Parameters and Fluxes from Satellite Data - HOAPS 4.0.* Satellite Application Facility on Climate Monitoring (CM SAF). Retrieved from `https://wui.cmsaf.eu/safira/action/viewDoiDetails?acronym=HOAPS{\_}V002` doi: 10.5676/EUM_SAF_CM/HOAPS/V002

Barker, S., Chen, J., Gong, X., Jonkers, L., Knorr, G., & Thornalley, D. (2015). Icebergs not the trigger for North Atlantic cold events. *Nature*, *520*(7547), 333–336. Retrieved from `https://doi.org/10.1038/nature14330` doi: 10.1038/nature14330

Barker, S., & Knorr, G. (2021). Millennial scale feedbacks determine the shape and rapidity of glacial termination. *Nature Communications*, *12*(1), 2273. Retrieved from `https://doi.org/10.1038/s41467-021-22388-6` doi: 10.1038/s41467-021-22388-6

Barker, S., Knorr, G., Vautravers, M. J., Diz, P., & Skinner, L. C. (2010). Extreme deepening of the Atlantic overturning circulation during deglaciation. *Nature Geoscience*, *3*(8), 567–571. Retrieved from `https://doi.org/10.1038/ngeo921` doi: 10.1038/ngeo921

Bauska, T. K., Marcott, S. A., & Brook, E. J. (2021). Abrupt changes in the global carbon cycle during the last glacial period. *Nature Geoscience*, *14*(2), 91–96. Retrieved from `https://doi.org/10.1038/s41561-020-00680-2` doi: 10.1038/s41561-020-00680-2

Bonfils, C. J. W., Santer, B. D., Fyfe, J. C., Marvel, K., Phillips, T. J., & Zimmerman, S. R. H. (2020). Human influence on joint changes in temperature, rainfall and continental aridity. *Nature Climate Change*, *10*(8), 726–731. Retrieved from `https://doi.org/10.1038/s41558-020-0821-1` doi: 10.1038/s41558-020-0821-1

Boot, A., von der Heydt, A. S., & Dijkstra, H. A. (2022). Effect of the Atlantic Meridional Overturning Circulation on atmospheric pCO$_{2}$ variations. *Earth System Dynamics*, *13*(3), 1041–1058. Retrieved from `https://esd.copernicus.org/articles/13/1041/2022/` doi: 10.5194/esd-13-1041-2022

Boot, A., von der Heydt, A. S., & Dijkstra, H. A. (2023, June). *AMOC MEW GRL.* [dataset]. Zenodo. doi: 10.5281/zenodo.8042693

Castellana, D., Baars, S., Wubs, F. W., & Dijkstra, H. A. (2019). Transition Probabilities of Noise-induced Transitions of the Atlantic Ocean Circulation. *Scientific Reports*, *9*(1), 20284. Retrieved from `https://doi.org/10.1038/s41598-019-56435-6` doi: 10.1038/s41598-019-56435-6

Caves, J. K., Jost, A. B., Lau, K. V., & Maher, K. (2016). Cenozoic carbon cycle

imbalances and a variable weathering feedback. *Earth and Planetary Science Letters*, *450*, 152–163. Retrieved from `https://www.sciencedirect.com/science/article/pii/S0012821X16303223` doi: https://doi.org/10.1016/j.epsl.2016.06.035

Cimatoribus, A. A., Drijfhout, S. S., & Dijkstra, H. A. (2014). Meridional overturning circulation: stability and ocean feedbacks in a box model. *Climate Dynamics*, *42*(1), 311–328. Retrieved from `https://doi.org/10.1007/s00382-012-1576-9` doi: 10.1007/s00382-012-1576-9

Dekker, M. M., von der Heydt, A. S., & Dijkstra, H. A. (2018). Cascading transitions in the climate system. *Earth System Dynamics*, *9*(4), 1243–1260. Retrieved from `https://esd.copernicus.org/articles/9/1243/2018/` doi: 10.5194/esd-9-1243-2018

Dijkstra, H. A. (2007, oct). Characterization of the multiple equilibria regime in a global ocean model. *Tellus A*, *59*(5), 695–705. Retrieved from `https://doi.org/10.1111/j.1600-0870.2007.00267.x` doi: https://doi.org/10.1111/j.1600-0870.2007.00267.x

Doedel, E. J., Paffenroth, R. C., Champneys, A. C., Fairgrieve, T. F., Kuznetsov, Y. A., Oldeman, B. E., ... Wang, X. J. (2007). *AUTO-07p: Continuation and Bifurcation Software for Ordinary Differential Equations.*

Drijfhout, S. (2015). Competition between global warming and an abrupt collapse of the AMOC in Earth's energy imbalance. *Scientific Reports*, *5*(1), 14877. Retrieved from `https://doi.org/10.1038/srep14877` doi: 10.1038/srep14877

Eyring, V., Bony, S., Meehl, G. A., Senior, C. A., Stevens, B., Stouffer, R. J., & Taylor, K. E. (2016, may). Overview of the Coupled Model Intercomparison Project Phase 6 (CMIP6) experimental design and organization. *Geosci. Model Dev.*, *9*(5), 1937–1958. Retrieved from `https://gmd.copernicus.org/articles/9/1937/2016/https://gmd.copernicus.org/articles/9/1937/2016/gmd-9-1937-2016.pdf` doi: 10.5194/gmd-9-1937-2016

Follows, M. J., Ito, T., & Dutkiewicz, S. (2006). On the solution of the carbonate chemistry system in ocean biogeochemistry models. *Ocean Modelling*, *12*(3), 290–301. Retrieved from `http://www.sciencedirect.com/science/article/pii/S1463500305000533` doi: https://doi.org/10.1016/j.ocemod.2005.05.004

Gottschalk, J., Battaglia, G., Fischer, H., Frölicher, T. L., Jaccard, S. L., Jeltsch-Thömmes, A., ... Stocker, T. F. (2019). Mechanisms of millennial-scale atmospheric CO2 change in numerical model simulations. *Quaternary Science Reviews*, *220*, 30–74. Retrieved from `http://www.sciencedirect.com/science/article/pii/S0277379118310473` doi: https://doi.org/10.1016/j.quascirev.2019.05.013

Held, I. M., & Soden, B. J. (2006). Robust Responses of the Hydrological Cycle to Global Warming. *Journal of Climate*, *19*(21), 5686–5699. Retrieved from `https://journals.ametsoc.org/view/journals/clim/19/21/jcli3990.1.xml` doi: 10.1175/JCLI3990.1

Jackson, L. C., Kahana, R., Graham, T., Ringer, M. A., Woollings, T., Mecking, J. V., & Wood, R. A. (2015). Global and European climate impacts of a slowdown of the AMOC in a high resolution GCM. *Climate Dynamics*, *45*(11), 3299–3316. Retrieved from `https://doi.org/10.1007/s00382-015-2540-2` doi: 10.1007/s00382-015-2540-2

Lenton, T. M., Held, H., Kriegler, E., Hall, J. W., Lucht, W., Rahmstorf, S., & Schellnhuber, H. J. (2008). Tipping elements in the Earth's climate system. *Proceedings of the National Academy of Sciences*, *105*(6), 1786–1793. Retrieved from `https://www.pnas.org/doi/abs/10.1073/pnas.0705414105` doi: 10.1073/pnas.0705414105

Lueker, T. J., Dickson, A. G., & Keeling, C. D. (2000). Ocean pCO2 calculated from dissolved inorganic carbon, alkalinity, and equations for K1 and K2: validation based on laboratory measurements of CO2 in gas and seawater at

equilibrium. *Marine Chemistry*, *70*(1), 105–119. Retrieved from `https://www.sciencedirect.com/science/article/pii/S0304420300000220` doi: https://doi.org/10.1016/S0304-4203(00)00022-0

Lynch-Stieglitz, J. (2017). The Atlantic Meridional Overturning Circulation and Abrupt Climate Change. *Annual Review of Marine Science*, *9*(1), 83–104. Retrieved from `https://doi.org/10.1146/annurev-marine-010816-060415` doi: 10.1146/annurev-marine-010816-060415

Marchal, O., Stocker, T. F., & Joos, F. (1998, jun). Impact of oceanic reorganizations on the ocean carbon cycle and atmospheric carbon dioxide content. *Paleoceanography*, *13*(3), 225–244. Retrieved from `https://doi.org/10.1029/98PA00726` doi: https://doi.org/10.1029/98PA00726

Matsumoto, K., & Yokoyama, Y. (2013, jun). Atmospheric Δ14C reduction in simulations of Atlantic overturning circulation shutdown. *Global Biogeochemical Cycles*, *27*(2), 296–304. Retrieved from `https://doi.org/10.1002/gbc.20035` doi: https://doi.org/10.1002/gbc.20035

McKay, D. I. A., Staal, A., Abrams, J. F., Winkelmann, R., Sakschewski, B., Loriani, S., . . . Lenton, T. M. (2022). Exceeding 1.5°C global warming could trigger multiple climate tipping points. *Science*, *377*(6611), eabn7950. Retrieved from `https://www.science.org/doi/abs/10.1126/science.abn7950` doi: 10.1126/science.abn7950

Millero, F. J. (1983). CHAPTER 43 - Influence of Pressure on Chemical Processes in the Sea. In J. P. RILEY & R. B. T. C. O. CHESTER (Eds.), (pp. 1–88). Academic Press. Retrieved from `https://www.sciencedirect.com/science/article/pii/B9780125886086500079` doi: https://doi.org/10.1016/B978-0-12-588608-6.50007-9

Mucci, A. (1983, sep). The solubility of calcite and aragonite in seawater at various salinities, temperatures, and one atmosphere total pressure. *American Journal of Science*, *283*, 780–799. Retrieved from `https://ui.adsabs.harvard.edu/abs/1983AmJS..283..780M` doi: 10.2475/ajs.283.7.780

Munhoven, G. (2013). Mathematics of the total alkalinity–pH equation - pathway to robust and universal solution algorithms: the SolveSAPHE package v1.0.1. *Geoscientific Model Development*, *6*(4), 1367–1388. Retrieved from `https://gmd.copernicus.org/articles/6/1367/2013/` doi: 10.5194/gmd-6-1367-2013

O'Neill, C. M., Hogg, A. M., Ellwood, M. J., Eggins, S. M., & Opdyke, B. N. (2019). The [simple carbon project] model v1.0. *Geoscientific Model Development*, *12*(4), 1541–1572. Retrieved from `https://gmd.copernicus.org/articles/12/1541/2019/` doi: 10.5194/gmd-12-1541-2019

Palter, J. B. (2015). The Role of the Gulf Stream in European Climate. *Annual Review of Marine Science*, *7*(1), 113–137. Retrieved from `https://doi.org/10.1146/annurev-marine-010814-015656` doi: 10.1146/annurev-marine-010814-015656

Rahmstorf, S. (2002). Ocean circulation and climate during the past 120,000 years. *Nature*, *419*(6903), 207–214. Retrieved from `https://doi.org/10.1038/nature01090` doi: 10.1038/nature01090

Schmittner, A., & Galbraith, E. D. (2008). Glacial greenhouse-gas fluctuations controlled by ocean circulation changes. *Nature*, *456*(7220), 373–376. Retrieved from `https://doi.org/10.1038/nature07531` doi: 10.1038/nature07531

Sinet, S., von der Heydt, A. S., & Dijkstra, H. A. (2023, jan). AMOC Stabilization Under the Interaction With Tipping Polar Ice Sheets. *Geophysical Research Letters*, *50*(2), e2022GL100305. Retrieved from `https://doi.org/10.1029/2022GL100305` doi: https://doi.org/10.1029/2022GL100305

Sun, Y., Knorr, G., Zhang, X., Tarasov, L., Barker, S., Werner, M., & Lohmann, G. (2022). Ice sheet decline and rising atmospheric CO2 control AMOC sensitivity to deglacial meltwater discharge. *Global and Planetary Change*, *210*, 103755.

Retrieved from https://www.sciencedirect.com/science/article/pii/S0921818122000224 doi: https://doi.org/10.1016/j.gloplacha.2022.103755

van der Ploeg, R., Cramwinckel, M. J., Kocken, I. J., Leutert, T. J., Bohaty, S. M., Fokkema, C. D., . . . Sluijs, A. (2023). North Atlantic surface ocean warming and salinization in response to middle Eocene greenhouse warming. *Science Advances*, *9*(4), eabq0110. Retrieved from https://www.science.org/doi/abs/10.1126/sciadv.abq0110 doi: 10.1126/sciadv.abq0110

Vellinga, M., & Wood, R. A. (2002). Global Climatic Impacts of a Collapse of the Atlantic Thermohaline Circulation. *Climatic Change*, *54*(3), 251–267. Retrieved from https://doi.org/10.1023/A:1016168827653 doi: 10.1023/A:1016168827653

Vellinga, M., & Wood, R. A. (2008). Impacts of thermohaline circulation shutdown in the twenty-first century. *Climatic Change*, *91*(1), 43–63. Retrieved from https://doi.org/10.1007/s10584-006-9146-y doi: 10.1007/s10584-006-9146-y

Weijer, W., Cheng, W., Drijfhout, S. S., Fedorov, A. V., Hu, A., Jackson, L. C., . . . Zhang, J. (2019, aug). Stability of the Atlantic Meridional Overturning Circulation: A Review and Synthesis. *Journal of Geophysical Research: Oceans*, *124*(8), 5336–5375. Retrieved from https://doi.org/10.1029/2019JC015083 doi: https://doi.org/10.1029/2019JC015083

Weijer, W., Cheng, W., Garuba, O. A., Hu, A., & Nadiga, B. T. (2020, jun). CMIP6 Models Predict Significant 21st Century Decline of the Atlantic Meridional Overturning Circulation. *Geophysical Research Letters*, *47*(12), e2019GL086075. Retrieved from https://doi.org/10.1029/2019GL086075 doi: https://doi.org/10.1029/2019GL086075

Weiss, R. F. (1974). Carbon dioxide in water and seawater: the solubility of a non-ideal gas. *Marine Chemistry*, *2*(3), 203–215. Retrieved from https://www.sciencedirect.com/science/article/pii/0304420374900152 doi: https://doi.org/10.1016/0304-4203(74)90015-2

Williams, R. G., & Follows, M. J. (2011). *Ocean Dynamics and the Carbon Cycle: Principles and Mechanisms*. Cambridge: Cambridge University Press. Retrieved from https://www.cambridge.org/core/books/ocean-dynamics-and-the-carbon-cycle/31EF28FEF48A172FF746B3E654F9455A doi: DOI:10.1017/CBO9780511977817

Wunderling, N., Donges, J. F., Kurths, J., & Winkelmann, R. (2021). Interacting tipping elements increase risk of climate domino effects under global warming. *Earth System Dynamics*, *12*(2), 601–619. Retrieved from https://esd.copernicus.org/articles/12/601/2021/ doi: 10.5194/esd-12-601-2021

Zeebe, R. E., Zachos, J. C., & Dickens, G. R. (2009). Carbon dioxide forcing alone insufficient to explain Palaeocene–Eocene Thermal Maximum warming. *Nature Geoscience*, *2*(8), 576–580. Retrieved from https://doi.org/10.1038/ngeo578 doi: 10.1038/ngeo578

Zhang, X., Knorr, G., Lohmann, G., & Barker, S. (2017). Abrupt North Atlantic circulation changes in response to gradual CO2 forcing in a glacial climate state. *Nature Geoscience*, *10*(7), 518–523. Retrieved from https://doi.org/10.1038/ngeo2974 doi: 10.1038/ngeo2974
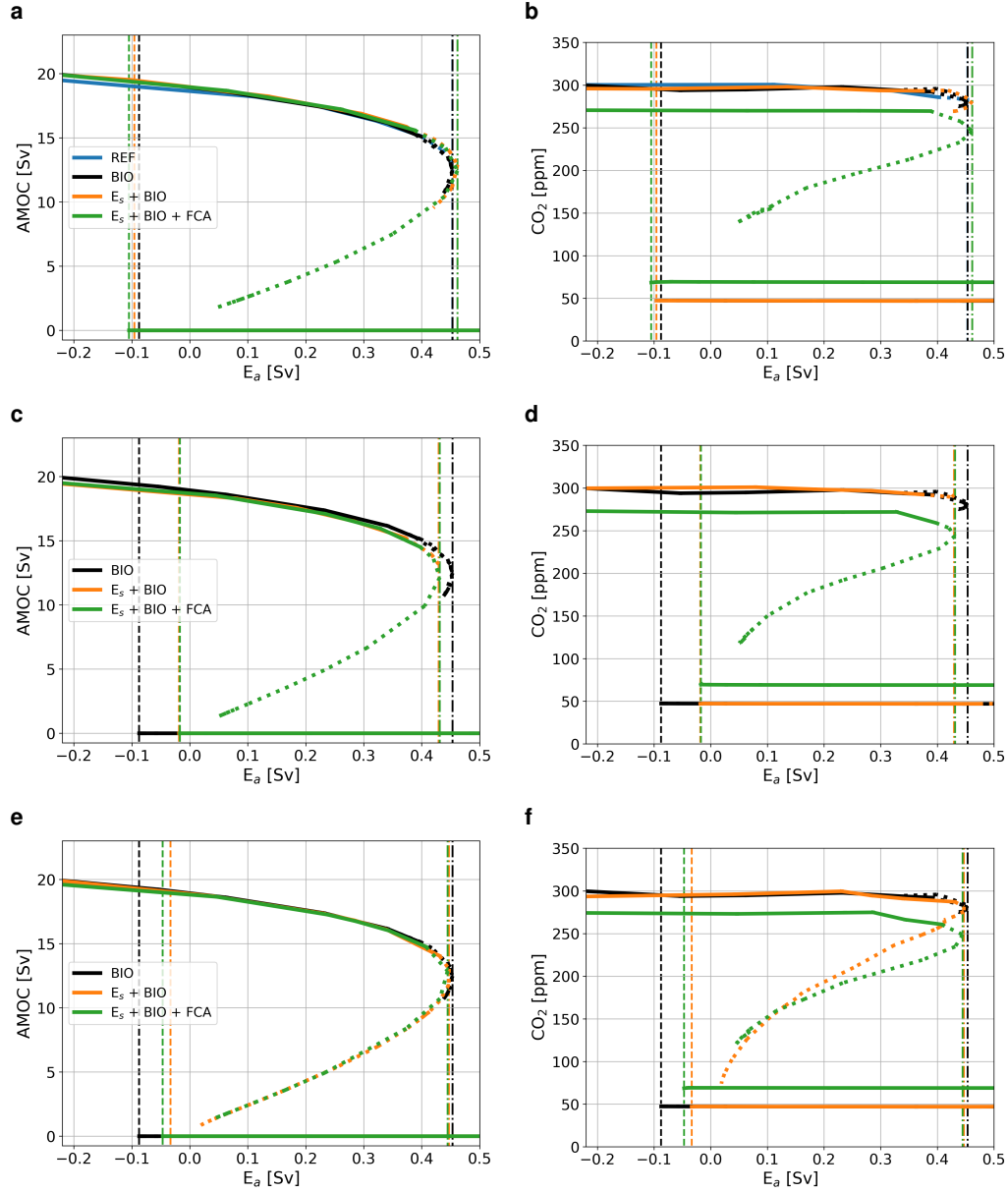
Figure 2. Bifurcation diagram showing the sensitivity of the AMOC to E_a. Solid lines represent stable steady state solutions, dotted lines represent unstable solutions, dash-dotted lines represent the location of the saddle node on the on-branch, and dashed lines the location of the saddle node on the off-branch. The blue lines represent a case without biological, E_s-pCO_2 and rain ratio coupling (REF), the black lines with only the biological coupling (BIO), the orange lines with the linear CMIP6 based E_s and biological coupling (E_s + BIO), and the green lines represent a case where also the rain ratio feedback is applied (E_s + BIO + FCA). Results are for the AMOC strength in Sv (a) and atmospheric pCO_2 in ppm (b). Case REF is difficult to see in A because it is similar to case BIO except that it does not simulate an off-branch. Panels a and b are for Eq. 1, panels c and d are for Eq. 2 and panels e and f are for Eq. 3. In a, b, c and d the orange saddle node lines are located behind the green lines.
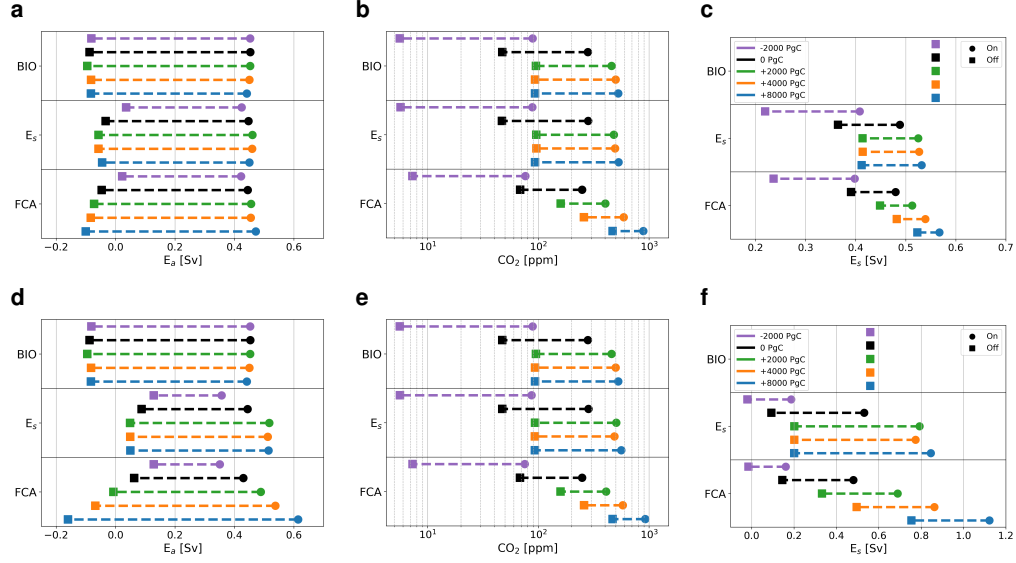
Figure 3. Panel a shows the location of the saddle nodes versus E_a in Sv, panel b shows the corresponding CO_2 concentration in ppm (note that the x-axis is logarithmic), and c shows the corresponding value of E_s in Sv following Eq. 2. In A-C the top of the figure represents case BIO, the middle case E_s + BIO, and the bottom case E_s + BIO + FCA. Square markers represent the location of the saddle node on the off-branch and round markers the location of the saddle node on the on-branch for cases where 4000 PgC is removed (purple), 2000 PgC is removed (black), the default carbon content (green), 4000 PgC is added (orange) and where 8000 PgC is added (blue) to the the standard case considered in Fig. 2. Panels d-f are as in a-c but for the E_s coupling in Eq. 3.
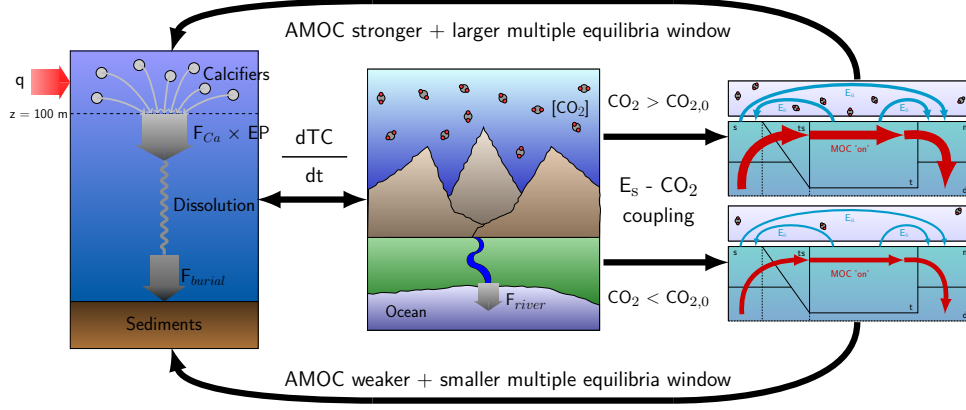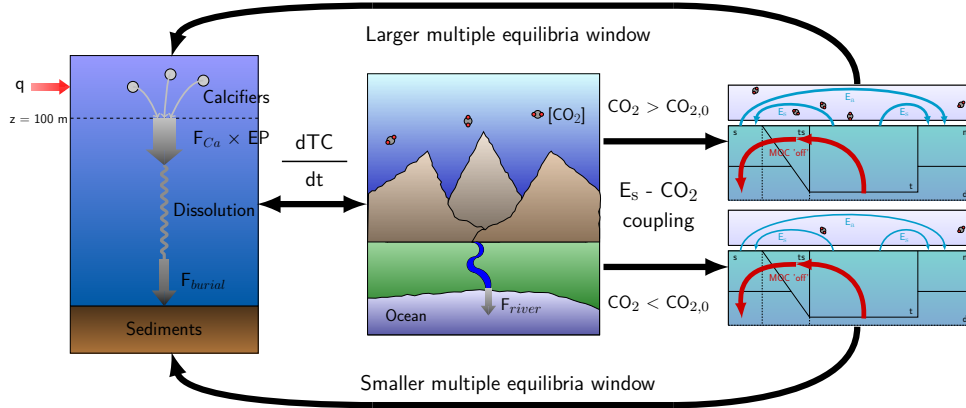
Figure 4. Illustrations of the main mechanisms affecting atmospheric pCO₂ and AMOC stability. Panel a shows the mechanisms for the on-branch. A strong AMOC increases export production through increased nutrient advection (left panel), which is accompanied by a high atmospheric pCO₂ due to the necessary balance between the river influx and sediment burial (middle panel). If the CO₂ concentration is larger (smaller) than CO₂,₀ than the AMOC will strengthen (weaken) and the MEW increases (decreases) (right panels). Panel b shows the mechanisms for the off-branch. The absence of an AMOC decreases export production through decreased nutrient advection (left panel), accompanied by a low atmospheric pCO₂ (middle panel). When pCO₂ is larger (smaller) than pCO₂,₀ the MEW increases (decreases) (right panel).